Ferroelectric properties of $Ba_xSr_{1-x}TiO_3$ solid solutions obtained by molecular dynamics simulation

2004 J. Phys.: Condens. Matter 16 3495

(http://iopscience.iop.org/0953-8984/16/20/019)

INSTITUTE OF PHYSICS PUBLISHING JOURNAL OF PHYSICS: CONDENSED MATTER

J. Phys.: Condens. Matter **16** (2004) 3495–3506 PII: S0953-8984(04)73317-2

Ferroelectric properties of $Ba_xSr_{1-x}TiO_3$ solid solutions obtained by molecular dynamics simulation

S Tinte[1,4], M G Stachiotti[1], S R Phillpot[2,3], M Sepliarsky[1,2], D Wolf[2] and R L Migoni[1]

[1] Instituto de Física Rosario, FCEIA, UNR, Rosario, Argentina
[2] Materials Science Division, Argonne National Laboratory, Argonne, IL 60439, USA
[3] Department of Materials Science and Engineering, University of Florida, Gainesville, FL 32611, USA

E-mail: sphil@mse.ufl.edu

Received 11 December 2003, in final form 9 March 2004
Published 7 May 2004
Online at stacks.iop.org/JPhysCM/16/3495
DOI: 10.1088/0953-8984/16/20/019

Abstract

Classical shell-model potentials for describing the complex ferroelectric behaviour of barium titanate and strontium titanate are developed and used to simulate $Ba_xSr_{1-x}TiO_3$ solid solutions. The temperature versus composition phase diagram is very well described and the local behaviour of the structure and polarization is analysed. It is shown that the ferroelectric properties of the solid solution can be understood in terms of the effects of average density and the local chemical environment. The experimentally observed static dielectric peak broadening around T_c at low x is reproduced in the simulation and seems to be related to the average volume rather than to the local chemical environment.

1. Introduction

The current keen interest in solid solutions of perovskite ferroelectrics is driven by the desire to create structures with properties unachievable in single-component materials. Prototypical solid solutions are $Ba_xSr_{1-x}TiO_3$ (BST), a solid solution of $BaTiO_3$ (BTO) and $SrTiO_3$ (STO), and $KTa_xNb_{1-x}O_3$, a solid solution of $KNbO_3$ and $KTaO_3$. Both solid solutions exist for the whole concentration range and are mixtures of a ferroelectric with an incipient ferroelectric.

In these materials, the phase transitions, usually sharp in single-component perovskite ferroelectrics, are much more diffuse as evidenced by the rather broad peak in the temperature dependence of the dielectric constant: this is often characterized as the 'diffuse phase transition' (DPT), the origin of which is not well understood. It was originally suggested that the material might contain domains of dimension of 100–1000 Å with varying composition, each with its

[4] Current address: Department of Physics and Astronomy, Rutgers University, Piscataway, NJ 08854, USA.

own dielectric response [1]. However, it now appears that the DPT is an intrinsic property of homogeneously disordered perovskites and does not require long-ranged compositional inhomogeneity [2, 3]. Recently, therefore, attention has focused on how a structure without long-range chemical inhomogeneity can support a DPT. Since a structure that is chemically homogeneous on large length scales can, nevertheless, still have variations in the short-length-scale local composition and environment, it is the dielectric responses to these variations that are now thought to give rise to the DPT.

In this paper, we characterize the structure and ferroelectric and dielectric properties of BST. First, we demonstrate that it is possible to develop classical shell models with potentials for BTO and STO, suitable for molecular dynamics simulations of disordered materials, that reproduce the specific phase behaviour and ferroelectric properties (section 2). Second, we use these potentials in atomic-level simulations to characterize the basic structure and ferroelectric properties of BST solid solutions (section 3). Finally, we elucidate the correlation between the dielectric properties of these solid solutions and the local structure (section 4). Our conclusions appear in section 5.

2. Shell-model potentials for barium titanate and strontium titanate

Barium titanate (BTO) has a perovskite structure and undergoes successive transitions from cubic to tetragonal to orthorhombic and rhombohedral phases with decreasing temperature [4]. Strontium titanate (STO) is an incipient ferroelectric with a large dielectric constant. It undergoes a transition from the cubic phase to an antiferrodistortive phase involving tilting of the TiO_6 octahedra at $\sim$105 K [5, 6]. From 105 K down to $\sim$50 K the temperature dependence of the static dielectric constant is Curie–Weiss-like with an extrapolated transition temperature of $\sim$36 K. However, this low temperature ferroelectric transition has not been observed; current understanding is that the transition is suppressed by the presence of zero-point motion, resulting in a 'quantum paraelectric state' at low temperatures [7]. While to realistically model the coupling between BTO and STO in solid solutions and superlattices, it is necessary to capture the antiferrodistortive transition, a description of the lower temperature quantum paraelectric state would be necessary only for studies of the very low Ba concentration limit at very low temperatures. Since this regime is not the focus of this study, we can ignore quantum effects.

We have previously shown that a shell model for $KNbO_3$ with isotropic oxygen polarizability, which was derived from an earlier anisotropic shell model, is able to describe very well the phase behaviour and ferroelectric properties of that material [8]. This isotropic shell model has essentially the same form as the traditional shell models used for other oxide systems, with the single exception that the core–shell interactions are anharmonic, containing fourth-order terms. These fourth-order terms have the effect of accommodating the large atomic polarizations associated with the ferroelectric distortions. In this work, we show that it is also possible to derive an isotropic shell model for $BaTiO_3$; the result is a model suitable for molecular dynamics (MD) simulations of disordered systems. In addition to being unsuitable for the simulation of disordered systems, a significant drawback of a previously developed anisotropic shell model for $BaTiO_3$ [9] is that the theoretically determined transition temperatures are much lower than in experiment. Here therefore, we implement an ad hoc procedure to improve the transition temperatures of the simulations for the isotropic model. The anisotropic shell model for BTO and both the anisotropic and isotropic shell models for $KNbO_3$ were parametrized from the energy surfaces associated with the ferroelectric distortions obtained from local density approximation (LDA) calculations. We previously found that the transition temperatures are associated with, although not in a simple and straightforward manner, the energy barriers obtained as a function of the ferroelectric mode amplitude. By

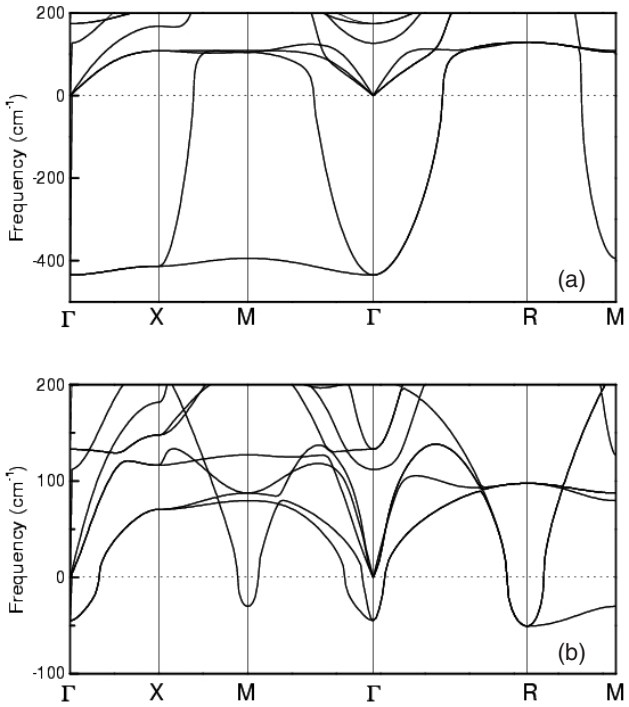

Figure 1. Phonon dispersion curves for the cubic phases of (a) $BaTiO_3$ and (b) $SrTiO_3$, calculated using the new isotropic shell-model potentials. The negative values correspond to imaginary frequencies, characteristic of the ferroelectric instability at the Γ point in $BaTiO_3$ and the additional antiferrodistortive instabilities at the R and M points in $SrTiO_3$.

construction, the previous anisotropic model for BTO yields instabilities and minima locations in the ferroelectric energetics rather similar to those obtained in LDA calculations, with energy lowerings of ∼1.2, 1.65 and 1.9 mRyd/cell for the [001], [011] and [111] ferroelectric mode displacements, respectively. As the experimentally determined transition temperatures are approximately twice as large as those obtained by our anisotropic simulations, here we parametrize the isotropic shell model such that the energy barriers are approximately twice as large as those obtained by LDA calculations. In this way the isotropic model developed for $BaTiO_3$ yields energy lowerings of ∼2.9, 3.8 and 4.5 mRyd/cell for the [001], [011] and [111] ferroelectric mode displacements, respectively. As we shall see, this does, indeed, have the desired effect of increasing the transition temperatures substantially. This result indicates that important unresolved issues may remain in the use of the LDA to describe ferroelectricity in perovskites [9, 10].

The phonon dispersion relations provide a global view of the harmonic energy surface around the cubic perovskite structure. In particular the unstable modes, which have imaginary frequencies, determine the nature of the phase transitions. The main features of the phonon dispersions of $BaTiO_3$ have been discussed previously in the context of the anisotropic shell model, where we showed that the anisotropic shell model agrees well with the *ab initio* linear response calculation of the phonon dispersion curves [9]. Figure 1(a) shows the low frequency phonon dispersion curves of cubic $BaTiO_3$ obtained with the isotropic model. The main features of the dispersion curves of the unstable modes are in good qualitative agreement with the *ab initio* linear response calculations [11]. However, the imaginary frequencies obtained with the model are twice as large as the LDA frequencies, which is consistent with the fact

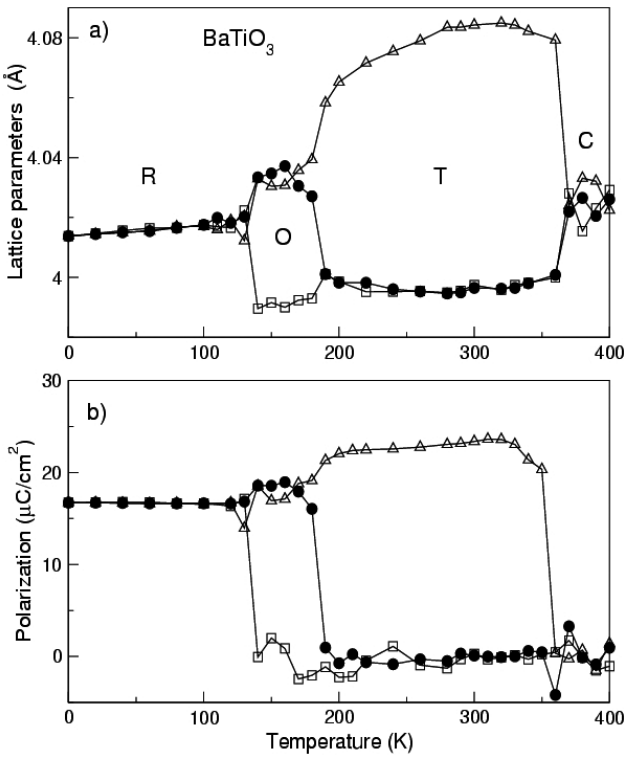

Figure 2. (a) The calculated phase diagram of $BaTiO_3$ shows the experimentally observed sequence of phase transitions. (b) The temperature dependence of the polarization is in reasonable agreement with experiment (see also table 1).

that the model energy barriers for the ferroelectric mode displacements are higher than those determined in the LDA.

In all of the constant-pressure molecular dynamics simulations described here we treat the Coulomb interactions using a direct summation method for the $1/r$ potential [12], which is conceptually simple, has been found to be easy to implement and is computationally robust and very efficient. Previously, we have successfully used this method for the simulation of ferroelectric behaviour in $KNbO_3$ [8, 13].

Figure 2(a) shows the phase diagram of BTO calculated using the isotropic shell model. Despite being a somewhat simpler model of the material than the anisotropic shell model, this isotropic shell model actually reproduces the transition temperatures of BTO much better due to the larger energy barriers. Like the anisotropic model, it displays the experimental observed sequence of rhombohedral, orthorhombic, tetragonal and cubic phases with increasing temperature and quite good agreement with the experimental lattice parameters (see table 1) [9]. However, in comparison with the anisotropic model, it gives transition temperature values (140, 190 and 360 K; see figure 2(a) and table 1) in better agreement with the experimental ones (183, 278 and 393 K). Nevertheless, the discrepancy for the computed orthorhombic–tetragonal transition temperature is significantly larger than for the other two transitions, thereby restricting the orthorhombic phase to a rather narrow temperature range. These transition temperatures are also much closer to experimental values than those obtained with the effective Hamiltonian model for BTO [14], which is also parametrized from LDA

Table 1. Structural parameters and Cartesian components of the spontaneous polarization for the different phases of $BaTiO_3$. For the orthorhombic phase, the equivalent pseudo-monoclinic cell parameters are reported.

Phase	Parameter	MD simulation	Experiment
Rhombohedral	a (Å)	4.016	4.003[a]
	α (deg)	89.67	89.84[a]
	P (μC cm^{-2})	16.6	13[a]–19[b]
	T_c (K)	140	183
Orthorhombic	a (Å)	3.991	3.987[a]
	$b = c$ (Å)	4.033	4.018[a]
	c/a	1.011	1.008
	P (μC cm^{-2})	18.5	14[a]–25[b]
	T_c (K)	190	278
Tetragonal	a (Å)	3.996	3.999[a]
	c (Å)	4.080	4.036[a]
	c/a	1.021	1.009
	P (μC cm^{-2})	22	17[a]–27[b]
	T_c (K)	360	393
Cubic	a (Å)	4.025	4.012[c]

[a] Reference [22].
[b] Reference [15].
[c] Reference [23].

calculations. Figure 2(b) shows the temperature dependence of the Cartesian components of the polarization. We see that the polarizations in the ferroelectric phases are rather similar to those observed experimentally (see table 1). For example, in the tetragonal phase at T_C (the cubic–tetragonal transition temperature) the z component is 22 μC cm^{-2}, compared with the experimentally measured value of 27 μC cm^{-2} [15].

In order to simulate BST, we have also parametrized an isotropic model for STO. From a computational point of view, this model must be compatible with the BTO model in that the only possible difference between the two lies in the different Ba–O and Sr–O interactions and the different polarizability parameters for Ba and Sr. The challenge is thus to reproduce, by only changing these interactions, the following main features of STO: (i) a smaller equilibrium volume; (ii) incipient ferroelectricity; and (iii) a tetragonal antiferrodistortive ground state. We found that these three critical features can, indeed, be reproduced. The equilibrium lattice constant of the resulting model in the cubic phase is $a = 3.90$ Å which reproduces the extrapolation to 0 K of the experimental lattice constant in the cubic phase. As regards the other two conditions, the low frequency phonon dispersion curves of the cubic structure are shown in figure 1(b). We find that the model reproduces the rather subtle antiferrodistortive instabilities, driven by the unstable modes at the R and M points. It also presents a subtle ferroelectric instability (unstable mode at the zone centre). These detailed features of the dispersion of the unstable modes along different direction in the Brillouin zone are in quite good agreement with *ab initio* linear response calculations [16].

Since our simulation technique is intrinsically classical, it should capture the low temperature phase that would be present in the absence of the quantum fluctuations. We find that at $T = 0$ K, STO is weakly tetragonal with $c/a = 1.0004$ (compared with the experimental value of 1.0009 near $T \sim 0$ K [17]). Consistent with experiment, in this tetragonal phase the oxygen octahedra are rotated in opposite senses in neighbouring cells,

which is a consequence of the antiferrodistortive instabilities displayed by the model in the phonon dispersion curves. This structure disappears rapidly with increasing cell volume. In addition to this antiferrodistorted structure, the ground state also displays a net polarization of $\sim 9\ \mu C\ cm^{-2}$ along the [111] direction. This zero-temperature ferroelectricity is quite unstable, with the polarization disappearing at $T = 20$ K due thermal fluctuations, while the antiferrodistortive phase remains stable above this temperature. It is interesting to note that in STO the experimentally observed softening of the ferroelectric mode would appear to extrapolate to zero frequency close to 36 K. Thus, a ferroelectric phase transition would be expected at ∼36 K classically; however, quantum fluctuations saturate the softening and no ferroelectric transition is observed.

From the above, we conclude that atomic-level simulations using isotropic shell models can well reproduce the phase behaviour and ferroelectric properties of both BTO and STO.

3. Structure and ferroelectric properties of BST

The parametrizations of the STO and BTO potentials, described above, can be adopted with no additional modifications to describe BST. In this way we can describe BST over the full range of composition and temperature with potentials which are both completely independent of composition and do not require knowledge of any properties of BST solid solutions.

We have prepared random solid solutions of $Ba_xSr_{1-x}TiO_3$ of various compositions in the range $x = 0$ (pure STO) to $x = 1$ (pure BTO). For this purpose, we considered simulation supercells where the A-sites of the $ATiO_3$ perovskite are randomly occupied by Ba and Sr ions, with their corresponding polarizability parameters and Ba–O and Sr–O interactions as in the pure materials. Results for supercells with periodic boundary conditions ranging from $6 \times 6 \times 6$ unit cells (containing 1080 ions) to $10 \times 10 \times 10$ (5000 ions) were compared: no significant system-size dependence in structure or properties was found. The results discussed here were obtained with $8 \times 8 \times 8$ unit cells (2560 ions).

3.1. Average properties of BST

Since BTO and STO are both rhombohedral at $T = 0$ K, the composition dependence of the zero-temperature structure can be characterized by the single lattice parameter, $a = b = c$ (figure 3(a)), the crystallographic angle associated with the rhombohedral distortion (figure 3(b)) and the magnitude of the polarization along one of the pseudo-cubic axes (figure 3(c)); these data show a rather smooth dependence of the properties on x. For very low x ($x < 0.1$), these may actually be modified by the quantum fluctuations omitted in our simulation approach.

The results of the simulations on the phase behaviour of BST are summarized in figure 4 (filled symbols connected by solid lines) as the concentration dependence of the transition temperatures. With increasing concentration of Sr (i.e., decreasing x), the Curie temperature decreases essentially linearly with x. We find that all four phases remain stable down to $x \sim 0.2$ at which the three transition temperatures essentially coincide. Below $x \sim 0.2$ only the cubic and rhombohedral phases appear in the phase diagram. These results are similar to the experimental data of Lemanov *et al* (open symbols and dotted lines in figure 4) [18], giving particularly good agreement with the concentration at which the tetragonal and orthorhombic phases disappear from the phase diagram. The above analyses demonstrate that the isotropic shell model can reproduce the basic features of the phase behaviour of BST, on a semi-quantitative basis. Given this success, we now turn to an atomic-level characterization of the structure and properties, a task that is very difficult experimentally.

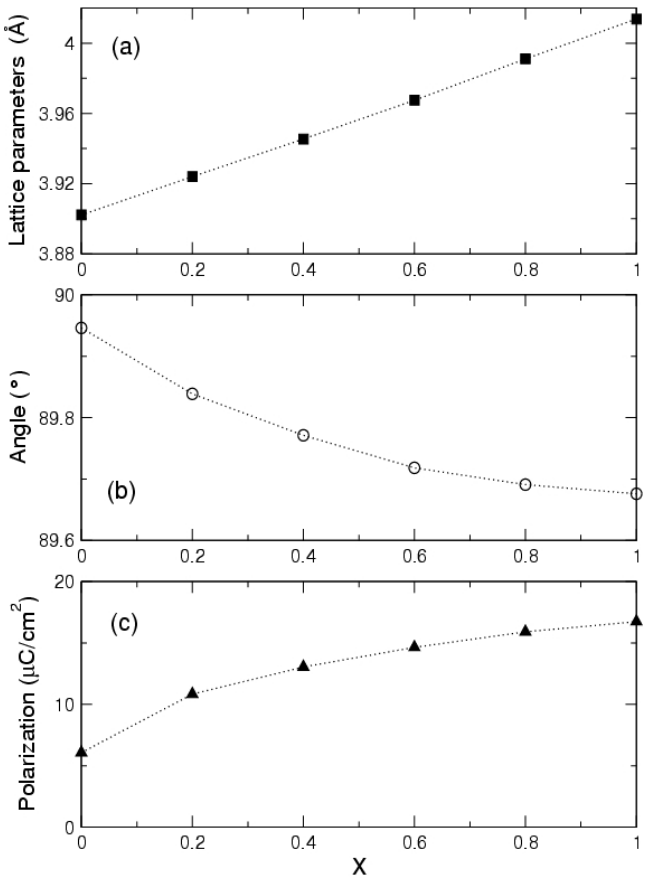

Figure 3. The dependence of the zero-temperature values of (a) the lattice parameter, (b) the crystallographic angle and (c) the polarization on x for $Ba_xSr_{1-x}TiO_3$.

3.2. Local structure and properties of BST

In this subsection, we analyse in some detail the atomic-level structure and polarization of the BST solid solutions. For these disordered ferroelectrics it is natural to analyse the local structure in terms of ⟨001⟩-oriented unit cells centred on either a Ba or a Sr ion, with the Ti ions at the corners and the O ions along the cell edges; we will refer to these as BTO and STO cells respectively.

There are two fundamental structural effects associated with the solid solution: a concentration dependence of the average volume and large variations in the local strain. The large (∼2.4%) mismatch in the zero-temperature lattice parameters of BTO and STO can introduce significant local strains in the solid solution, as illustrated in figure 5, which shows the nearest neighbour A–A distances (i.e., Ba–Ba, Sr–Sr and Ba–Sr) for $x = 0.2$. The Ba–Ba and Sr–Sr nearest neighbour distances display very similar unimodal distributions peaked around the average lattice parameter (compare with figure 3(a)). By contrast, the Sr–Ba spacing is bimodal with a minimum at the peak in the Ba–Ba and Sr–Sr spacings. This distribution arises from the rather different displacements Δ_{Ba} and Δ_{Sr} of the Ba and Sr ions, respectively, from their lattice sites. In the $T = 0$ K rhombohedral phase, they are directed along one of the ⟨111⟩ directions. The average distance between ions, d, is a consequence of the average atomic

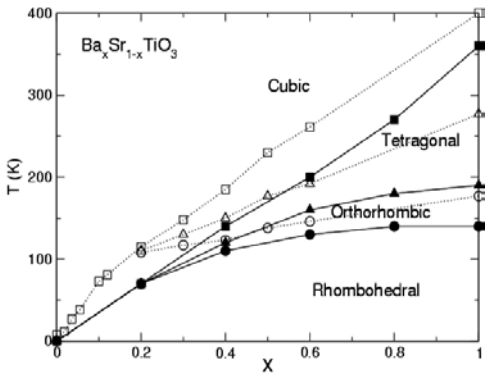

Figure 4. The concentration dependence of the transition temperatures as determined from figure 3 and related simulations (solid symbols and dark lines) shows good agreement with experimental values (open symbols and dotted lines).

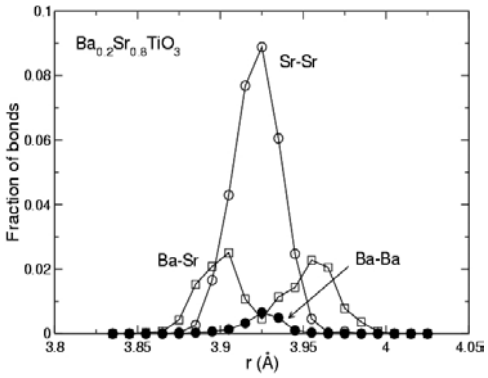

Figure 5. The distribution of A–A' nearest neighbour distances for $x = 0.2$ shows the bimodal distribution in the Ba–Sr separations. Other values of x yield similar distributions.

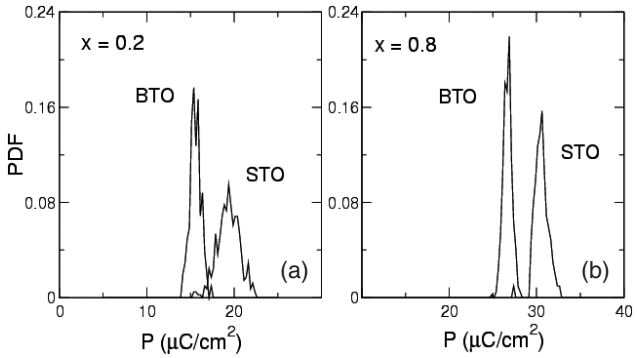

Figure 6. Polarization distribution functions (PDFs) for unit cells centred on a Sr ion (STO cells) and on a Ba ion (BTO cells) for (a) $x = 0.2$ and (b) $x = 0.8$ can be understood in terms of the average volume and the local environment.

volume. However, while $d_{\mathrm{Ba-Ba}} \sim d_{\mathrm{Sr-Sr}} \sim d$, $d_{\mathrm{Ba-Sr}}$ can take on the values $d + (\Delta_{\mathrm{Ba}} - \Delta_{\mathrm{Sr}})$ and $d - (\Delta_{\mathrm{Ba}} - \Delta_{\mathrm{Sr}})$; i.e., a bimodal distribution.

Figure 6 shows the distribution in the zero-temperature polarization for the BTO and STO cells for $x = 0.2$ and 0.8 concentrations, for each of which the tensile strain on the STO cells is sufficiently large to completely suppress the antiferrodistortive state. The most important effect here is associated with the strain. As indicated in figure 3, STO is denser than BTO. Thus in the solid solution, the STO cells tend to be under a tensile strain (which tends to encourage a ferroelectric distortion) while the BTO cells tend to be under a compressive strain (which tends to suppress the ferroelectric distortion). Indeed, the large tensile strain on the STO cells does have the effect of inducing a polarization in the system. Remarkably, for both compositions, the polarization of the STO cells is actually larger than that of the BTO cells.

There is also an additional effect associated with the local environment of each unit cell. In particular, we find that the maximum and minimum values of polarization for the STO cells correspond to the polarizations of STO cells (of the same average volume as the solid solution) embedded completely in a matrix of STO cells and BTO cells respectively. Likewise, for the

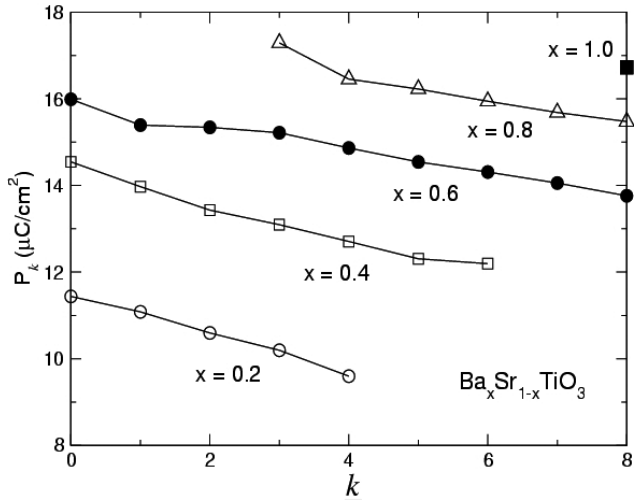

Figure 7. The average polarization at $T = 0$ K for Ti-centred unit cells containing Ba ions at k of the eight corners for various values of the composition shows the effect of the local environment.

BTO cells the maximum and minimum polarizations correspond to STO and BTO embeddings respectively.

The difference in average polarization of the BTO and STO cells observed in figure 6 could be related to a difference in the atomic displacements of Ba and Sr ions, which allowed us also to explain the bimodal Ba–Sr distance distribution observed in figure 5. In fact, the smaller ionic radius of Sr compared with Ba could allow a larger displacement of Sr relative to the oxygen sublattice. This phenomenon is represented in our model by a less repulsive Sr–O short-range interaction. In order to verify quantitatively whether this explains the observed difference in polarization we perform calculations of the atomic relaxations along the [111] direction for both $BaTiO_3$ and $SrTiO_3$, both with the shell model and with the LAPW electronic structure method [19], we consider a cubic cell with volume fixed to the average value in the $x = 0.8$ solid solution ($a = 3.99$ Å). (The polarizations are estimated from the displacement of atom i in the j direction, $d_i(j)$, and the effective ionic charges as $P_i = 1/a^3 \Sigma_j Z^*_{\text{eff}}(j) d_i(j)$. In each of the two methods employed, we use the corresponding values of effective charges.) With both methods, we obtain a larger polarization value for $SrTiO_3$: 47 and 36 μC cm^{-2} for the LAPW and model calculations against 39 and 32 μC cm^{-2} in the case of $BaTiO_3$. The largest contribution to the difference comes from the displacement of Sr relative to the oxygen cage (see table 2). This test with the LAPW calculations allows us also to again confirm that the shell model correctly captures the physics involved in the local polarizations of this complex system.

The above arguments have shown qualitatively the effects of the volume and local structure on the polarization. To make the role of the local structure on polarization more explicit we define P_k as the average of a single Cartesian component of the polarization of all *Ti-centred* unit cells containing k ($k = 0, 1, 2, \ldots, 8$) Ba ions at the corners for various compositions. From figure 7, we see clearly that there is an approximately linear decrease in the polarization with k, exactly the behaviour we would expect from a traditional rule of mixtures.

The above analyses show that, since the average polarization is largely determined by the concentration dependent volume, its trend with Ba content is opposite to the one observed for the local polarization variations at fixed volume. Thus, increasing the Ba concentration

Table 2. Components along the z-axis of [111] atomic displacements, in units of the lattice parameter, for cubic cells of BTO and STO with $a = 3.99$ Å, corresponding to the average lattice parameter for the $x = 0.8$ random solid solution. The results in the first line are from LAPW calculations, while those in second line are from shell model calculations.

	$BaTiO_3$	$SrTiO_3$
A	−0.0018 (LAPW)	−0.0112 (LAPW)
	−0.0003 (shell model)	−0.0124 (shell model)
Ti	−0.0125	−0.0147
	−0.0109	−0.0081
O_z	0.0094	0.0123
	0.0069	0.0101
O_{xy}	0.0158	0.0152
	0.0160	0.0201

increases the volume of the system and increases the average polarization. Nevertheless, for any given Ba concentration, the greater the number of Ba ions at the corners of a Ti-centred unit cell, the smaller the polarization of that individual unit cell.

4. Dielectric properties and the diffuse phase transition

The main reason that disordered ferroelectrics are attracting so much attention is the tunability of their dielectric properties. For example, in pure BTO the peak in the dielectric behaviour is at the Curie temperature, $T_c = 393$ K, associated with the cubic–tetragonal phase transition. By forming a solid solution with STO this transition temperature, and hence the peak in the dielectric behaviour, can be shifted down to any convenient value. Simultaneously, for certain compositions this has the additional advantage of broadening the transition, thereby increasing substantially the temperature range over which an enhanced dielectric response can be obtained. As a measure of the dielectric properties of these disordered ferroelectrics we have determined the zero-frequency real dielectric constant, as a function of temperature for $x = 0.2$, 0.8 and 1.

The dielectric properties are determined from the change in polarization on the application of an external electric field. We then calculate the dielectric constant from the usual continuum electrodynamics relation between the electric field and polarization, $\varepsilon_{zz} = \partial P_z/\partial E_z + 1$. By performing simulations at various values of the electric field we have verified the linear dependence of the polarization on field up to $\sim$50 kV cm^{-1} for a range of x and temperature. For the dielectric constant calculations described below we use $E = 20$ kV cm^{-1}, which is well within this linear response regime.

The temperature dependence of the dielectric constants for BTO and for BST with $x = 0.8$, 0.2 are shown in figure 8. In BTO we see the rather sharp peak in the dielectric constant at the cubic–tetragonal phase transition of $T = 360$ K, and smaller enhancements in the dielectric constant at the tetragonal–orthorhombic and orthorhombic–rhombohedral phase transitions at $T = 190$ and 140 K respectively. For $x = 0.8$, the peak in the dielectric constant associated with the cubic–tetragonal phase transition is shifted down in temperature (see also figure 4), but the height and width of the peak in the dielectric constant are very similar to those for BTO. In this regard, BST with $x = 0.8$ behaves as a normal ferroelectric.

The situation for $x = 0.2$, i.e., $Ba_{0.2}Sr_{0.8}TiO_3$, is much more complicated. Of course, the peak is shifted further down in temperature to reflect the reduction in T_c seen in figure 4. Significantly more interesting, however, is that the peak is now extremely broad with a long tail above the transition temperature. This behaviour is exactly what is observed experimentally. The origin of the broad peak in the dielectric constant at low concentrations cannot be explained as an effect of the atomic local environment. The model yields an almost linear dependence of

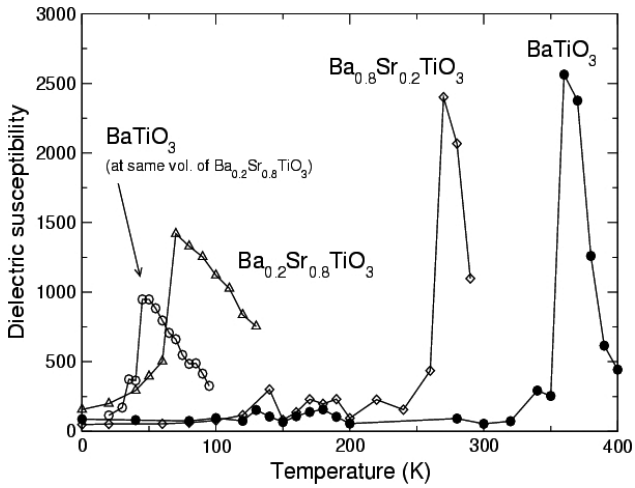

Figure 8. The zero-frequency dielectric susceptibility, ε, as a function of temperature for $BaTiO_3$ and for $x = 0.8$ and 0.2 shows the diffuse phase transition at low x. The dielectric constant for pure $BaTiO_3$ at the volume corresponding to the $x = 0.23$ random solid solution also shows a broad peak, demonstrating that the diffuse phase transition arises largely from volume effects.

the transition temperature as a function of concentration. On the other hand, the differences in local polarization between BTO and STO cells for a given concentration are rather small. These features indicate that the material could be considered as a compositionally homogeneous system, where local inhomogeneities would not play an important role in broadening the dielectric constant peak. Consequently, we have performed simulations for pure $BaTiO_3$ at the volume of the solid solution with $x = 0.2$. The dielectric constant also displays a broad peak similar to the one obtained for the solid solution. This is an indication that the diffuseness is a cell volume effect. This is consistent with the results of Zhang *et al* [20], whose Ising-like model calculations showed that T_c is correlated with the cell volume in $Sr_xBa_{1-x}TiO_3$ irrespective of the origin of volume variation: be it A-site ion substitution or mechanical pressure, its effect on T_c is the same. They subsequently argued that the order and diffuseness of the phase transition does not originate from local compositional fluctuations, but is related to the cell volume [21], as in the case of T_c.

We recall that the ferroelectric instability becomes weaker with decreasing unit-cell volume and at a sufficient volume reduction is destroyed entirely. This is associated with decreases in the depths and increases in the widths of the potential wells related to the ferroelectric distortions. Naturally, such wide and shallow potential wells make the ferroelectric phases dielectrically soft over a much wider temperature range.

5. Conclusions

We have demonstrated that atomic-level simulations using an isotropic shell model can reproduce the structure, phase behaviour and ferroelectric properties of barium and strontium titanate and their solid solutions in a semi-quantitative manner. We have also demonstrated the ability of atomic-level simulation to divide the properties of solid solutions of these materials into ones related to the average strain on the system and ones related to the local environment.

Specifically, we find that the ferroelectric properties of the solid solution are determined mainly by the cell volume. We have also shown that a random solid solution, without large inhomogeneities in the composition, can lead to a broad peak in the dielectric behaviour.

Acknowledgments

This work was supported by the US Department of Energy, Office of Science, under Contact W-31-109-Eng-38, by the DOE S&P Center Project on Nanoscale Phenomena in Perovskite Thin Film, and by CONICET—Argentina. ST gratefully acknowledges the hospitality of Argonne National Laboratory during the period in which much of this work was performed.

References

[1] Smolenskii G A 1970 *J. Phys. Soc. Japan* **28** 26
[2] Hochli U T, Knorr K and Loidl A 1990 *Adv. Phys.* **39** 599
[3] Tiwari V S, Singh N and Pandey D 1995 *J. Phys: Condens. Matter* **7** 1441
[4] Jona F and Shirane G 1993 *Ferroelectric Crystals* (New York: Dover)
[5] Fleury P A, Scott J F and Worlock J M 1968 *Phys. Rev. Lett.* **21** 16
[6] Shirane G and Yamada Y 1969 *Phys. Rev.* **177** 858
[7] Muller K A and Burkhard H 1979 *Phys. Rev.* B **19** 3593
Muller K A, Berlinger W and Tosatti E 1991 *Z. Phys.* B **84** 277
[8] Sepliarsky M, Phillpot S R, Wolf D, Stachiotti M G and Migoni R L 2000 *Appl. Phys. Lett.* **76** 3986
[9] Tinte S, Stachiotti M G, Sepliarsky M, Migoni R L and Rodríguez C O 1999 *J. Phys.: Condens. Matter* **11** 9679
[10] Tinte S, Íñiguez J, Rabe K M and Vanderbilt D 2003 *Phys. Rev.* B **67** 064106
[11] Ghosez P H, Gonze X and Michenaud J-P 1998 *Ferroelectrics* **206** 205
[12] Wolf D, Keblinski P, Phillpot S R and Eggebrecht J 1999 *J. Chem. Phys.* **110** 8254
[13] Sepliarsky M, Phillpot S R, Streiffer S K, Stachiotti M G and Migoni R L 2001 *Appl. Phys. Lett.* **79** 4417
[14] Zhong W, Vanderbilt D and Rabe K M 1994 *Phys. Rev. Lett.* **73** 1861
[15] Shirane G and Takeda A 1952 *J. Phys. Soc. Japan* **7** 1
[16] Lasota C, Wang C-Z, Yu R and Krakauer H 1997 *Ferroelectrics* **194** 109
[17] Heidemann A and Wettengel H 1973 *Z. Phys.* **258** 429
[18] Lemanov V V, Smirnova E P, Syrnikov P P and Tarakanov E A 1996 *Phys. Rev.* B **54** 3151
[19] Blaha P, Schwarz K, Dufek K P and Augustyn R 1997 *WIEN97* Technical University of Vienna
Improved and updated Unix version of the original copyrighted WIEN-code, which was published by
Blaha P, Schwarz K, Sorantin P and Trickey S B 1990 *Comput. Phys. Commun.* **59** 399
[20] Zhang L, Zhong W L, Wang Y G and Zhang P L 1997 *Solid State Commun.* **104** 263
[21] Zhang L, Zhong W L, Wang G L, Zhang P L and Wang Y G 1999 *J. Phys. D: Appl. Phys.* **32** 546
[22] Kwei G H, Lawson A C, Billinge S J L and Cheong S-W 1993 *J. Phys. Chem.* **97** 2368
[23] Kay H F and Vousden P 1949 *Phil. Mag.* **40** 1019